Mon. Not. R. Astron. Soc. **000**, 1–10 (2014) Printed 15 January 2014 (MN LATEX style file v2.2)

On the baryon acoustic oscillation amplitude as a probe of radiation density

Will Sutherland[1⋆] & Lukasz Mularczyk[1]
[1] *School of Physics and Astronomy, Queen Mary University of London, Mile End Road, London E1 4NS, UK*

arXiv:1401.3240v1 [astro-ph.CO] 14 Jan 2014

MNRAS: Accepted 2013 December 13. Received 2013 December 12; in original form 2013 July 4

ABSTRACT

The baryon acoustic oscillation (BAO) feature in the distribution of galaxies has been widely studied as an excellent standard ruler for probing cosmic distances and expansion history, and hence dark energy. In contrast, the amplitude of the BAO feature has received relatively little study, mainly due to limited signal-to-noise, and complications due to galaxy biasing, effects of non-linear clustering and dependence on several cosmological parameters. As expected, the amplitude of the BAO feature is sensitive to the cosmic baryon fraction: for standard radiation content, the cosmic microwave background (CMB) acoustic peaks constrain this precisely and the BAO amplitude is largely a redundant cross-check. However, the CMB mainly constrains the redshift of matter-radiation equality, $z_{\rm eq}$, and the baryon/photon ratio: if a non-standard radiation density ($N_{\rm eff}$) is allowed, increasing $N_{\rm eff}$ while matching the CMB peaks leads to a reduced baryon fraction and a lower relative BAO amplitude. We construct an observable for the relative area of the BAO feature from the galaxy correlation function (Eq. 8); from linear-theory models, we find that this is mainly sensitive to $N_{\rm eff}$ and quite insensitive to other cosmological parameters. More detailed work from N-body simulations will be needed to constrain the effects of non-linearity and scale-dependent galaxy bias on this observable.

Key words: cosmic background radiation – cosmological parameters – cosmology:theory – large-scale structure of Universe.

1 INTRODUCTION

The detection of baryon acoustic oscillations (BAOs) in the large-scale distribution of galaxies in both the SDSS (Eisenstein et al 2005) and 2dFGRS (Cole et al 2005) redshift surveys was a major milestone for cosmology, strongly supporting the standard paradigm for structure formation based on gravitational instability including cold (or warm) dark matter. Recently, there have been several new independent measurements of the BAO feature in galaxy redshift surveys, e.g. from SDSS-DR8 (Percival et al 2010), WiggleZ (Blake et al 2011), 6dFGRS (Beutler et al 2011), an angular measurement from SDSS-DR9 (Seo et al 2012), and a first measurement from BOSS (Anderson et al 2012), which are all consistent with the concordance ΛCDM model at the few-percent level.

The BAO feature in galaxy clustering (Peebles & Yu 1970; Bond & Efstathiou 1984; Eisenstein & Hu 1998; Meiksin, White & Peacock 1999) has a very similar origin to the acoustic peaks in the cosmic microwave background (CMB) temperature power spectrum. Most recent attention has focused on the length-scale of the BAO feature, used as a standard ruler to measure cosmic distances in units of the sound horizon $r_s(z_d)$ at the baryon drag epoch. Many theoretical and computational studies (Seo et al 2008, 2010) have concluded that the comoving length-scale of the BAO feature evolves by $\sim 0.5\,\%$ between the CMB era and the recent past $z \sim 0.3$ due to the non-linear growth of structure, but this shift can be corrected down to the $0.1\,\%$ level using reconstruction methods (Eisenstein et al 2007; Padmanabhan et al 2012). Therefore, the BAO feature is probably the best-understood standard ruler in the moderate-redshift universe, and when combined with CMB observations it offers great power for probing the cosmic expansion history and therefore the properties of dark energy (Weinberg et al 2013). These BAO distance measurements are complementary to those from type-Ia supernovae, have potentially smaller systematic errors, and can offer direct information on the time-variable $H(z)$ without differentiation. On the downside, cosmic variance sets a floor on the BAO precision in the low-redshift universe, ~ 1 percent at

⋆ E-mail: w.j.sutherland@qmul.ac.uk

© 2014 RAS

$z \sim 0.25$ and worsening below this (Seo & Eisenstein 2007) .

However, in this paper we look at a different property, specifically the overall amplitude of the BAO feature, rather than the length-scale. As expected, the amplitude is mainly sensitive to the cosmic baryon fraction (relative to total matter), f_b. Until now, the BAO amplitude has received much less attention than the length-scale, for two main reasons: firstly, recent CMB results from WMAP (Hinshaw et al 2012), SPT (Keisler et al 2011; Story et al 2013) and ACT (Sievers et al 2013) measure the baryon fraction to around 4 percent relative precision (given standard assumptions), while the strongest detection of the BAO peak (Anderson et al 2012) gives $\sim 6\sigma$ significance or $\sim 16\%$ error in amplitude. Secondly, complications due to galaxy bias, the non-linear growth of structure, redshift-space distortions and the uncertain global shape of the power spectrum make it challenging to extract the baryon fraction from the BAO feature, even with very large future redshift surveys.

However, we note that parameter estimates from the CMB are subject to a significant degeneracy between f_b and the total radiation density in the CMB era, usually parametrized by an effective number of neutrino species $N_{\rm eff}$. Recent reviews of $N_{\rm eff}$ are given by e.g. Riemer-Sorensen, Parkinson & Davis (2013a) and Abazajian et al (2012).

In contrast, the BAO feature is sensitive to the baryon fraction rather directly: therefore, combining CMB measurements (primarily sensitive to the physical baryon density ω_b and the redshift of matter-radiation equality $z_{\rm eq}$) with a BAO measurement sensitive to f_b may provide an interesting probe of the radiation density, $N_{\rm eff}$. This may be less precise than other methods, but is largely complementary.

The plan of the paper is as follows: in § 2 we review the main effects of varying cosmological parameters, including f_b and radiation density, on CMB and BAO observations. In § 3 we present numerical predictions of the BAO feature for a set of models (selected to give a good match to WMAP) with varying matter density and $N_{\rm eff}$, and we derive a statistic based on the galaxy correlation function which is sensitive to f_b and $N_{\rm eff}$, but cancels galaxy bias and dark energy to leading order. We summarize our conclusions in § 4. Most of this work was completed before the *Planck* release in March 2013, so we mainly use WMAP-9 fit parameters (Hinshaw et al 2012) as our baseline. The adjustments post-*Planck* are moderate, and we discuss the implications of recent *Planck* results (Planck Collaboration, Ade et al (2013)) in § 3.3.

Throughout the paper we use the standard notation that Ω_i is the present-day density of species i relative to the critical density; and the physical density $\omega_i \equiv \Omega_i h^2$, with $h \equiv H_0/(100\,{\rm km\,s^{-1}\,Mpc^{-1}})$.

2 BAOS, RADIATION DENSITY $N_{\rm eff}$ AND THE COSMIC BARYON FRACTION

2.1 Overview of BAOs

The BAO feature appears as a single hump in the galaxy correlation function $\xi(r)$, or equivalently a series of decaying wiggles in the power spectrum (see Eisenstein, Seo & White (2007) for a clear explanation in real space, and Bassett & Hlozek (2010) and Weinberg et al (2013) for reviews). The length-scale of the hump is very close to the comoving sound horizon $r_s(z_d)$ at the baryon drag epoch $z_d \simeq 1020$; this z_d is commonly defined by the fitting formula Eq. 4 of Eisenstein & Hu (1998). (This formula is defined for standard $N_{\rm eff}$; however the dependence of z_d on $N_{\rm eff}$ is weak, so the error from adopting the fitting formula is small). This comoving length is predicted precisely mainly from CMB constraints, and several very large redshift surveys are ongoing or planned to exploit this as a standard ruler to measure cosmic distances at $0.2 \lesssim z \lesssim 2.5$ and thus probe dark energy.

Standard cosmological models contain a density of collisionless dark matter $\sim 5\times$ larger than the baryon density. This explains naturally why the acoustic peaks in the CMB power spectrum have large relative amplitude, while the BAO feature is relatively weak in the late-time galaxy correlation function. Qualitatively, this occurs because the acoustic peaks at last scattering appeared only in the power spectrum of baryons, not dark matter: the peaks are prominent in the CMB because almost all CMB photons last scattered off a free electron. After decoupling, the distribution of baryons and dark matter became averaged together by gravitational growth of structure over the next few e–foldings between the CMB era and redshift $z \sim 20$ (Eisenstein, Seo & White 2007), well before the formation of large galaxies. The dark matter dominates in this averaging, so the BAO signal in the galaxy correlation function becomes diluted by a factor $\sim f_b$. In the following we define the baryon fraction as

$$f_b \equiv \frac{\omega_b}{\omega_c + \omega_b} \tag{1}$$

so that the denominator includes CDM and baryons, but excludes massive neutrinos.

Thus, the BAO peak amplitude provides a potential measure of the baryon fraction; this has been used as a simple and compelling argument against MOND-type modified gravity theories without non-baryonic dark matter (Dodelson 2011).

We can make this more quantitative and use the BAO feature to directly estimate the cosmic baryon fraction. However, there are several reasons why this has received little attention to date:

(i) Recent observations of the CMB power spectrum (Hinshaw et al 2012) measure the physical baryon density ω_b to ≈ 2 percent precision, and (assuming standard $N_{\rm eff}$), measure the physical matter density ω_m to 3 percent; the errors on these are weakly correlated, so this gives an estimate of the cosmic baryon fraction f_b to $\leqslant 4$ percent relative precision. (Recent results from the *Planck* mission have improved this to the ~ 2 percent level, see § 3.3).

(ii) The BAO feature is affected by several effects: it is blurred by the non-linear growth of structure, and amplified by galaxy bias, which is challenging to measure and may also be scale-dependent.

(iii) The overall large-scale shape of the galaxy power spectrum also depends on other cosmological parameters, and this will also have some influence on the BAO peak shape.

Thus, at first sight it appears that BAOs cannot compete in precision with the CMB as a probe of f_b. This is partly true, but with an important caveat: the CMB-based estimates of f_b are significantly degenerate with the total radiation density in the CMB era.

2.2 Radiation density

At this point we define our notation on densities: as usual, we define the parameter $N_{\rm eff}$ such that the radiation density at matter-radiation equality is

$$\rho_{rad} = \rho_\gamma (1 + 0.2271\, N_{\rm eff}) \quad (2)$$

where ρ_{rad}, ρ_γ are densities of (total) radiation and photons respectively. Here $N_{\rm eff}$ is an "effective" number of neutrinos, but in fact it is not specific to neutrinos and counts any species (except photons) which were relativistic until around matter-radiation equality. Assuming the standard population of only three very light neutrinos with the oscillation parameters given by solar, atmospheric and beam-based neutrino experiments, the value of $N_{\rm eff}$ can be accurately predicted as $N_{\rm eff} = 3.046$ (Mangano et al 2005); here the additional 0.046 arises from a small residual coupling of neutrinos to baryons and photons at the epoch of electron/positron annihilation.

It is also convenient to define the scaled radiation density $X_{\rm rad}$ by

$$X_{\rm rad} \equiv \frac{\rho_{rad}}{1.6918\, \rho_\gamma} = 1 + 0.134\, (N_{\rm eff} - 3.046) \quad (3)$$

where the factor of 1.6918 is the bracket in Eq. 2 for $N_{\rm eff} = 3.046$; therefore $X_{\rm rad} = 1.00$ for standard radiation content, and for example $X_{\rm rad} = 1.134$ for $N_{\rm eff} = 4.046$, i.e. the case of additional "dark radiation" with energy density equal to one standard neutrino flavour. Here $N_{\rm eff}$ and $X_{\rm rad}$ are equivalent, but the latter is convenient later since several parameters of interest scale almost as half-integer powers of $X_{\rm rad}$.

There are now several known routes to probe $N_{\rm eff}$ from observations: historically it was first constrained by big bang nucleosynthesis, (Steigman, Schramm & Gunn 1977; Mangano & Serpico 2011). However, ^{4}He is the nuclide with the main sensitivity to $N_{\rm eff}$, and observational measurements of the primordial ^{4}He abundance, Y_P, appear to be limited by systematic errors; over the past 25 years the estimates of Y_P have shifted significantly upwards, but the realistic error bars have not much improved. Unless a new better method of measuring Y_P can be found, we cannot expect dramatic progress from the Helium route. Recently, a constraint on $N_{\rm eff}$ has been derived from deuterium abundance (Pettini & Cooke 2012), but this currently relies on only a single object, and also uses the baryon density derived from the CMB.

Secondly, the CMB damping tail at high multipoles $\ell \gtrsim 1400$ is sensitive to $N_{\rm eff}$ (Jungman et al 1996; Bashinsky & Seljak 2003; Hou et al 2013); and several recent measurements (Hou et al 2012;Riemer-Sorensen, Parkinson & Davis 2013a; Ade et al 2013) give tantalizing but not decisive hints for a value higher than the standard 3.046. However, the CMB damping tail method is significantly degenerate with other possible new parameters, including running of the spectral index n_s and non-standard helium abundance Y_P (Hou et al 2013; Joudaki 2013), so other complementary probes of $N_{\rm eff}$ are desirable.

Thirdly, combining CMB data with a direct local measurement of H_0 can also probe $N_{\rm eff}$; however, using CMB+H_0 alone is critically dependent on other assumptions such as $w = -1$ and flatness. An improvement on the H_0 method is given by Sutherland (2012), who showed that a *theory-free* measurement of r_s can be obtained by combining a low-z BAO redshift survey and a suitable absolute distance measurement to a matched redshift (specifically $4\overline{z}/3$, where $\overline{z}$ is the characteristic redshift of the BAO survey). This almost cancels the distance effects from dark energy and curvature; comparing such a direct r_s measurement to CMB data (which mainly constrains $r_s\sqrt{X_{\rm rad}}$ rather than r_s alone) therefore probes $N_{\rm eff}$. The above-mentioned method is less theory-dependent than the CMB damping tail, but requires a challenging measurement of a distance to $z \sim 0.3$ to ~ 2 percent absolute accuracy.

We will demonstrate below that the amplitude of the BAO feature provides a fourth possible probe of $N_{\rm eff}$: this is currently much less precise than the known methods above, but involves different assumptions and systematics; with future massive redshift surveys expected in the next decade, it may provide a useful complement to the better-known methods above.

2.3 Cosmological parameter set

The present-day photon density $\omega_\gamma = \Omega_\gamma h^2$ is very well constrained by the observed CMB temperature (Fixsen 2009) and spectrum to be $\omega_\gamma \simeq 1/40440$; and we define $\omega_{cb} \equiv \omega_c + \omega_b$ to be the physical matter density today, specifically CDM and/or WDM plus baryons, excluding neutrinos. Defining $z_{\rm eq}$ as the redshift of matter-radiation equality, and simply assuming that the photon density scales with redshift as $\propto (1+z)^4$, and matter conservation so CDM and baryon densities scale $\propto (1+z)^3$ (i.e. no decaying dark matter, dark energy to dark matter transitions, or other exotic effects) leads to the following identities:

$$\omega_{cb} = \frac{(1 + z_{\rm eq})\, X_{\rm rad}}{23904} \quad (4)$$

$$h = \sqrt{\frac{(1 + z_{\rm eq})\, X_{\rm rad}}{23904\, \Omega_{cb}}} \quad (5)$$

$$f_b \equiv \frac{\omega_b}{\omega_{cb}} = \frac{23904\, \omega_b}{(1 + z_{\rm eq})\, X_{\rm rad}} \quad (6)$$

The equations above are independent of assumptions about dark energy and flatness. They remain valid for the case of small non-zero neutrino mass, $m_\nu \lesssim 0.3\,$eV: since our definition of Ω_{cb} excludes the contribution from massive neutrinos today, while neutrinos this light were almost fully relativistic at the era of matter-radiation equality. This assumption is reasonable given recent upper limits on neutrino mass from CMB+galaxy clustering data (Ade et al 2013; Giusarma et al 2013; Riemer-Sorensen, Parkinson & Davis 2013b). Clearly, low-mass neutrinos are matter-like at $z \lesssim 100$ and do contribute to Ω_m in late-time observables, but we treat Ω_ν as a separate contribution.

We now choose a basic 6+1 set of cosmological parameters as

$$z_{\rm eq};\ \Omega_{cb};\ \omega_b;\ A;\ n_s;\ \tau;\ X_{\rm rad} \tag{7}$$

where the first three and $X_{\rm rad}$ are defined above, as usual A is the scalar perturbation amplitude (which cancels in the following), n_s is the scalar spectral index and τ is the optical depth to last scattering. Then, h, ω_{cb} and f_b are derived parameters from Eqs. (4)–(6). We may add optional parameters, curvature Ω_k, dark energy equation of state w and present-day neutrino density Ω_ν defaulting to $0, -1, \approx 0.0013$ respectively (for minimal neutrino mass). Then $\Omega_{tot} \equiv 1 - \Omega_k$, and the dark energy density Ω_{DE} is another derived parameter, via $\Omega_{DE} = 1 - \Omega_{cb} - \Omega_k - \Omega_\nu$.

This parameter set (7) including $z_{\rm eq}$ and Ω_{cb} in the basic six looks unconventional compared to the more common choice including ω_m, Ω_{DE} as two of the basic parameters; but for variable $N_{\rm eff}$, our set links more naturally to observational constraints as we will see below; see also Appendix A, and the discussion in Section 4.2 of Sutherland (2012). To summarize the latter, dimensionless observables such as the CMB acoustic wavenumber ℓ_*,[1] and distance ratios from BAO and SNe provide good constraints on dimensionless parameters including $z_{\rm eq}$ and Ω_{cb}; but there remains one overall scale degeneracy between $N_{\rm eff}$ and dimensionful parameters such as H_0, t_0, ρ_{cb}. (Parameters such as h, ω_{cb} are only pseudo-dimensionless since they are relative to an arbitrary choice of $100\,{\rm km\,s^{-1}\,Mpc^{-1}}$, and these are affected by this degeneracy).

It has been shown by several authors (Hu & Sugiyama 1996; Jungman et al 1996; Bashinsky & Seljak 2003; Jimenez et al 2004; Komatsu et al 2011) that the heights of the first few acoustic peaks in the CMB primarily constrain the redshift of matter-radiation equality $z_{\rm eq}$, *not* the physical matter density ω_{cb}.[2] These latter two parameters are equivalent if we force $N_{\rm eff} \simeq 3.04$, but if we allow $N_{\rm eff}$ to be free they are no longer equivalent, and then $z_{\rm eq}$ is constrained much better than ω_{cb} by CMB data (see e.g. Komatsu et al 2011).

The WMAP data also constrains the baryon density ω_b accurately. The effect of baryons on the CMB derives mainly from the baryon/photon ratio; given the photon density measured very accurately by COBE (Fixsen 2009), the ω_b estimate from WMAP is only weakly dependent on $N_{\rm eff}$ or $X_{\rm rad}$.

Measuring both ω_b and $z_{\rm eq}$ immediately gives us the product $f_b\,X_{\rm rad}$ from Eq. 6; so, the key point from the above is that the first few CMB acoustic peaks provide an accurate constraint on the product $f_b\,X_{\rm rad}$, but f_b and $X_{\rm rad}$ are significantly degenerate. Therefore, adding a non-CMB observable which is sensitive to f_b can provide another probe of $N_{\rm eff}$.

In the next section, we show that the relative amplitude of the BAO peak in galaxy clustering may provide such a test: it depends mainly on f_b, with weak sensitivity to other parameters. Thus, comparing a BAO-based estimate of f_b to a CMB-based measurement (approximately $f_b X_{\rm rad}$) can provide a new probe of the radiation density which is largely independent of existing methods. A strong point of this method is that the CMB can measure $z_{\rm eq}$ using only the first three acoustic peaks; for models near concordance parameter values, the ratio of the third to first peak height is especially sensitive to $z_{\rm eq}$ (Hu et al 2001; Page et al 2003), and the third peak at $\ell \approx 800$ is only weakly affected by Silk damping which dominates at $\ell \gtrsim 1500$. Thus, while we need CMB data at $\ell < 1000$, this method is not strongly dependent on the CMB damping tail and other possible early-time nuisance parameters.

3 ESTIMATING BARYON FRACTION FROM THE BAO PEAK

3.1 The BAO equivalent width

We noted above that the CMB power spectrum from WMAP constrains $f_b X_{\rm rad}$ to ~ 4 percent, (and this improves to $\sim 2\%$ with *Planck* data); therefore, an estimate of f_b derived from the BAO amplitude can translate into a probe of $X_{\rm rad}$ or equivalently $N_{\rm eff}$.

However, deriving f_b from the BAO feature is affected by several complications listed below: firstly there is galaxy bias, which may be scale-dependent. Here we choose to work with the correlation function rather than the power spectrum, since the former makes the BAO feature a single hump which simplifies the analysis. In the linear-bias approximation, the galaxy and matter correlation functions are related by $\xi_{gg}(r) \simeq b^2 \xi_{mm}(r)$, therefore a suitable ratio of correlation functions near the BAO bump vs outside the bump can cancel galaxy bias if it is scale-independent. This is believed to be a good approximation at linear scales $k < 0.1\,h\,{\rm Mpc}^{-1}$ (Angulo et al 2008; Baugh 2013), but a better understanding of galaxy formation may be required to clarify this.

Secondly, the BAO bump is blurred by the non-linear growth of structure, mainly due to peculiar motions (Eisenstein et al 2007); this both lowers its height and broadens its shape, and causes a small shift in central position. However, it is shown by Orban & Weinberg (2011) that non-linear growth almost conserves the total area of the bump; thus, measuring the bump *area* rather than its height is relatively insensitive to the non-linear growth of structure.

Thirdly, the global shape of $\xi(r)$, with r in $h^{-1}\,{\rm Mpc}$ units, depends on other quantities including Ω_m and dark energy equation of state, which are not tightly constrained by the CMB. However, we show later that if we define $u = r/r_s$ to be the ratio of comoving separation r to the sound horizon scale, then the broad-band shape of $\xi(u)$ on intermediate scales depends mostly on $z_{\rm eq}$: nearly all shape dependence on other parameters is collapsed into $z_{\rm eq}$, which is already well determined by the CMB.

Therefore, we define the following observable W_b from the measured galaxy correlation function ξ_{gg}, as a measure of the BAO "equivalent width": we define

$$W_b \equiv \frac{\int_{u_3}^{u_4} u^2\,[\xi_{gg}(u) - \xi_{nb}(u)]\,du}{\int_{u_1}^{u_2} u^2\,\xi_{gg}(u)\,du} \tag{8}$$

where $\xi_{gg}(u)$ is the observed galaxy correlation function in

[1] Here, following WMAP convention, $\ell_* \equiv \pi/\theta_*$, with acoustic angle $\theta_* \equiv r_S(z_*)/(1+z_*)D_A(z_*)$ and z_* is the redshift of decoupling.

[2] Strictly, it is the ratio $(1+z_{\rm eq})/(1+z_*)$ which is important in the CMB, where z_* is the decoupling redshift; however in practice the relative uncertainty in z_* is much smaller than in $z_{\rm eq}$, so we ignore this for simplicity.

units of $u \equiv r/r_b$, r_b is the bump scale (here the value of r at the peak in $r^2\xi_{gg}(r)$), and $\xi_{nb}(u)$ is a smooth "no bump" curve, here a polynomial fitted to the regions of $\xi_{gg}(u)$ just outside the BAO bump. Then $u_1, \ldots, u_4$ are arbitrary dimensionless limits of integration, where u_3, u_4 span almost the full area of the bump; while u_1, u_2 are intermediate scales non-overlapping with the bump, used for normalization. There is a compromise here, since we want to avoid the non-linear regime $u_1 \lesssim 0.15$, while at $u_1 \gtrsim 0.6$ the measurement noise in $u^2\xi(u)$ generally increases, and becomes more sensitive to systematic errors. In the following we choose $u_1 = 1/3, u_2 = 2/3$ as simple values which give a well-measured signal in the linear regime, and are not too far below the bump scale to minimise the possible effects of scale-dependent bias.

In the above definition, a constant bias in ξ_{gg} cancels out as long as it is scale-independent on large scales $r \gtrsim 30\,h^{-1}$ Mpc; while a multiplicative stretch of cosmic distance scales (e.g. from varying dark energy) also cancels in W_b, since we are measuring at fixed fractions of the comoving scale r_b which is fitted from the data. The ratio between r_s and the horizon size at matter-radiation equality is determined almost entirely by $z_{\rm eq}$, so we expect W_b defined as above to be mainly sensitive to the baryon fraction f_b as desired.

To verify this and test parameter dependences, we next evaluate W_b from the linear matter power spectrum for some example theoretical models generated by CAMB.[3]

3.2 Dependence of W_b on $N_{\rm eff}$ and $z_{\rm eq}$

Here, we evaluate W_b (defined above) for a set of six representative models which are all consistent with CMB data up to 2012. All models are flat ΛCDM ($\Omega_{tot} = 1$, $w = -1$), and have n_s fixed to 0.96 and $\omega_b = 0.0226$ in accordance with WMAP. We vary $z_{\rm eq}$ and $N_{\rm eff}$, and also adjust Ω_{cb} to preserve the CMB acoustic scale ℓ_*.

For our "base" model (hereafter C3) we set $N_{\rm eff} = 3.046$, $z_{\rm eq} = 3264$, $\Omega_{cb} = 0.279$; therefore $\omega_{cb} = 0.1366$ and $h = 0.700$. For model C4 we add a fourth light neutrino species, but retain identical values of $z_{\rm eq}$ and Ω_{cb}; therefore C4 has ω_{cb} and h increased by 13.4% and 6.5% respectively relative to C3. (Here ω_b is held at 0.0226 for both models, so model C4 has dark matter density ω_c increased by slightly more than 13.4%, while f_b is reduced by a factor of 0.882).

The overall shape of the correlation function also depends significantly on $z_{\rm eq}$: to explore this dependence, we choose two models (labelled L3, L4) with $z_{\rm eq}$ fixed to 5% lower than C3, and respectively $N_{\rm eff} = 3.04$ and 4.04; likewise another two models (H3, H4) with $z_{\rm eq}$ fixed 5% higher than C3. For these models, Ω_{cb} is adjusted in order to preserve the CMB acoustic scale $\ell_* \equiv \pi/\theta_*$. The resulting parameter values are shown in Table 1. Since these models are all flat, they do not quite follow the CMB geometrical degeneracy, but they do follow the related degeneracy of constant ℓ_* or horizon angle as outlined in Percival et al (2002).

We used CAMB to evaluate the CMB temperature power spectra for the above six models; these are shown in Figure 1, normalized to match model C3 at $\ell = 100$. Clearly the CMB spectra are very similar for all our models, since the acoustic scales are matched by construction, and the variations in $z_{\rm eq}$ are only ±5 percent. Minor differences are apparent, notably around the third peak (which is positively correlated with $z_{\rm eq}$), while the effects of $N_{\rm eff}$ appear mainly in the damping tail and are small at $\ell < 1000$. We repeat here that $\omega_b = 0.0226$ and $n_s = 0.96$ have been held fixed in all models for simplicity, in order to highlight the effects of $z_{\rm eq}$ and $N_{\rm eff}$. Clearly, allowing n_s and ω_b to float to fit CMB data would result in model spectra that are even more similar, especially if a running spectral index is also allowed.

We took the linear-theory matter power spectra for the above six models generated by CAMB, and then Fourier transformed them to obtain the real-space matter correlation functions; these are shown in Figure 2, with the $x-$axis in units of h^{-1} Mpc corresponding to the observable from a low-z redshift survey.

For the matter correlation functions in Figure 2, the differences between models are much more obvious than in the CMB: the position of the BAO bump (in h^{-1} Mpc units) is insensitive to $N_{\rm eff}$ for fixed $z_{\rm eq}, \Omega_{cb}$, but it does shift with $z_{\rm eq}$. In fact, as explained in Appendix A, the BAO bump location is more sensitive to Ω_{cb} than $z_{\rm eq}$; but changing $z_{\rm eq}$ required us to adjust Ω_{cb} to conserve the CMB acoustic scale, and it is actually the change in Ω_{cb} which dominates the shift of the bump location. The other notable feature in Figure 2 is that all the $N_{\rm eff} = 4.04$ models have a slightly reduced BAO peak amplitude, as qualitatively expected given their smaller f_b.

To highlight the effects of varying $N_{\rm eff}$, in Figure 3 we plot the matter correlation functions as a function of $u = r/r_b$, so that the BAO bump appears at $u = 1$. This Figure shows clearly that the bump amplitude is mainly sensitive to $N_{\rm eff}$, while the broad-band shape (the ratio of power at $u \sim 0.2$ to that at $u \gtrsim 0.6$) is governed mainly by $z_{\rm eq}$. This is understandable since the broad-band shape is determined by the scale of the turnover in the matter power spectrum, which is directly proportional to the particle horizon size at $z_{\rm eq}$. This scale in observable h^{-1} Mpc units depends on several cosmological parameters. However, as noted in e.g. Eq. B2 of Sutherland (2012), the *ratio* of the BAO sound horizon $r_s(z_d)$ to the particle horizon r_H at $z_{\rm eq}$ (both in comoving units) has a simpler dependence: this ratio is well approximated by simply

$$\frac{r_s(z_d)}{r_H(z_{\rm eq})} \simeq 1.275 \left(\frac{1+z_{\rm eq}}{3201}\right)^{0.75} \quad ; \qquad (9)$$

since the sound speed $c_s(z)$ is well constrained by the WMAP baryon density. The dependence on other parameters such as Ω_{cb}, h, $X_{\rm rad}$ is almost entirely compressed into $z_{\rm eq}$, and the ratio is completely independent of late-time parameters such as w, Ω_k. Thus the changes in $\xi(u)$ in Figure 3 are largely driven by the differing $z_{\rm eq}$ and f_b between the six models, and adding optional parameters such as Ω_k, w will have minimal effect.

Here it is also noteworthy that the zero-crossing in $\xi(u)$ occurs close to $u \sim 1.2$ for all the models; this offers an interesting possible consistency test for the ΛCDM framework which is largely insensitive to galaxy bias. However, this is observationally challenging to measure since the zero-crossing is much more sensitive than the BAO bump posi-

[3] We used the 2011 January release of CAMB, by A. Lewis and A. Challinor, available from `http://camb.info/`

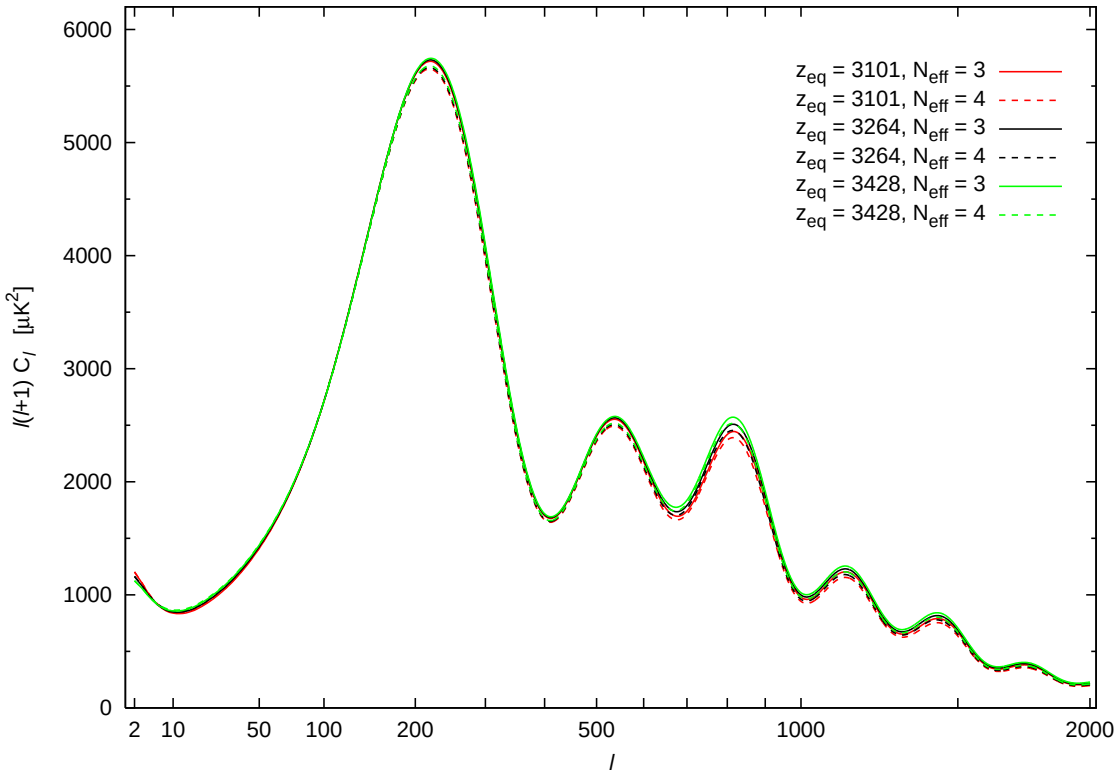

Figure 1. This figure shows the CMB temperature power spectra for the six example models from Table 1; all are normalized to match model C3 at $\ell = 100$. The horizontal axis is linear in $\sqrt{\ell}$ for improved resolution at low ℓ. Models with $N_{\rm eff} = 3.04$ are solid lines; models with $N_{\rm eff} = 4.04$ are dashed lines. The values of $z_{\rm eq}$ are labelled.

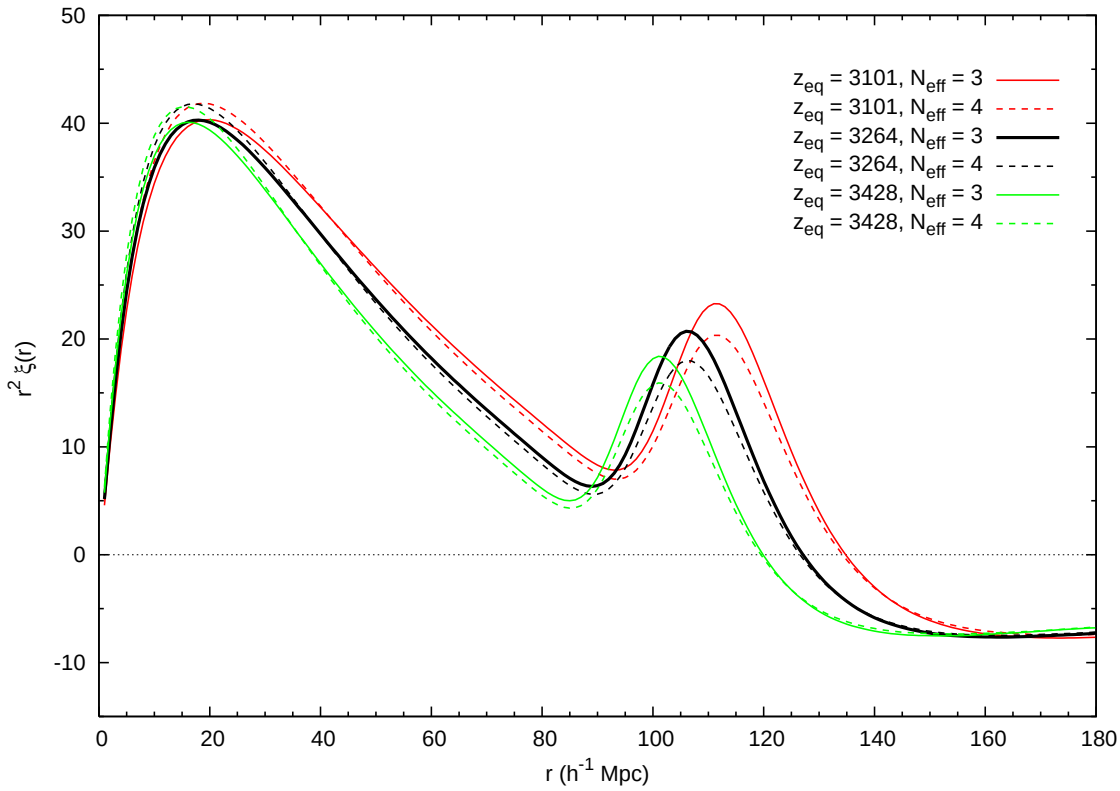

Figure 2. This figure shows the linear-theory matter correlation function for the six example models from Table 1; the ordinate is $r^2\xi_{mm}(r)$ for clarity. Models with $N_{\rm eff} = 3.04$ are solid lines; models with $N_{\rm eff} = 4.04$ are dashed lines. The thick solid line is model C3 ; the L and H models are respectively higher/lower at $r \sim 50\,h^{-1}$ Mpc.

Model	$z_{\rm eq}$	Ω_{cb}	$N_{\rm eff}$	ω_{cb}	f_b	H_0 ($\rm km\,s^{-1}\,Mpc^{-1}$)	W_b
L3	3101	0.247	3.04	0.1298	0.174	72.5	0.612
L4	3101	0.247	4.04	0.1471	0.154	77.1	0.561
C3	**3264**	**0.279**	**3.04**	**0.1366**	**0.165**	**70.0**	**0.614**
C4	3264	0.279	4.04	0.1549	0.146	74.5	0.561
H3	3428	0.315	3.04	0.1434	0.158	67.5	0.608
H4	3428	0.315	4.04	0.1626	0.139	71.9	0.560

Table 1. Cosmological parameters for the six example models discussed in the text. All models have $\Omega_{tot} = 1$, $w = -1$ and $\omega_b = 0.0226$. Model C3 (bold) is our baseline, while model C4 has $N_{\rm eff} = 4.04$ but unchanged $z_{\rm eq}$ and Ω_{cb}. Models labelled L and H have $z_{\rm eq}$ forced respectively 5% lower/higher than C, then Ω_{cb} adjusted to preserve the CMB acoustic scale. Values of ω_{cb}, f_b and H_0 are derived from the first three. The last column gives the value of W_b as defined in Eq. 8, calculated by integrating the linear-theory matter correlation function.

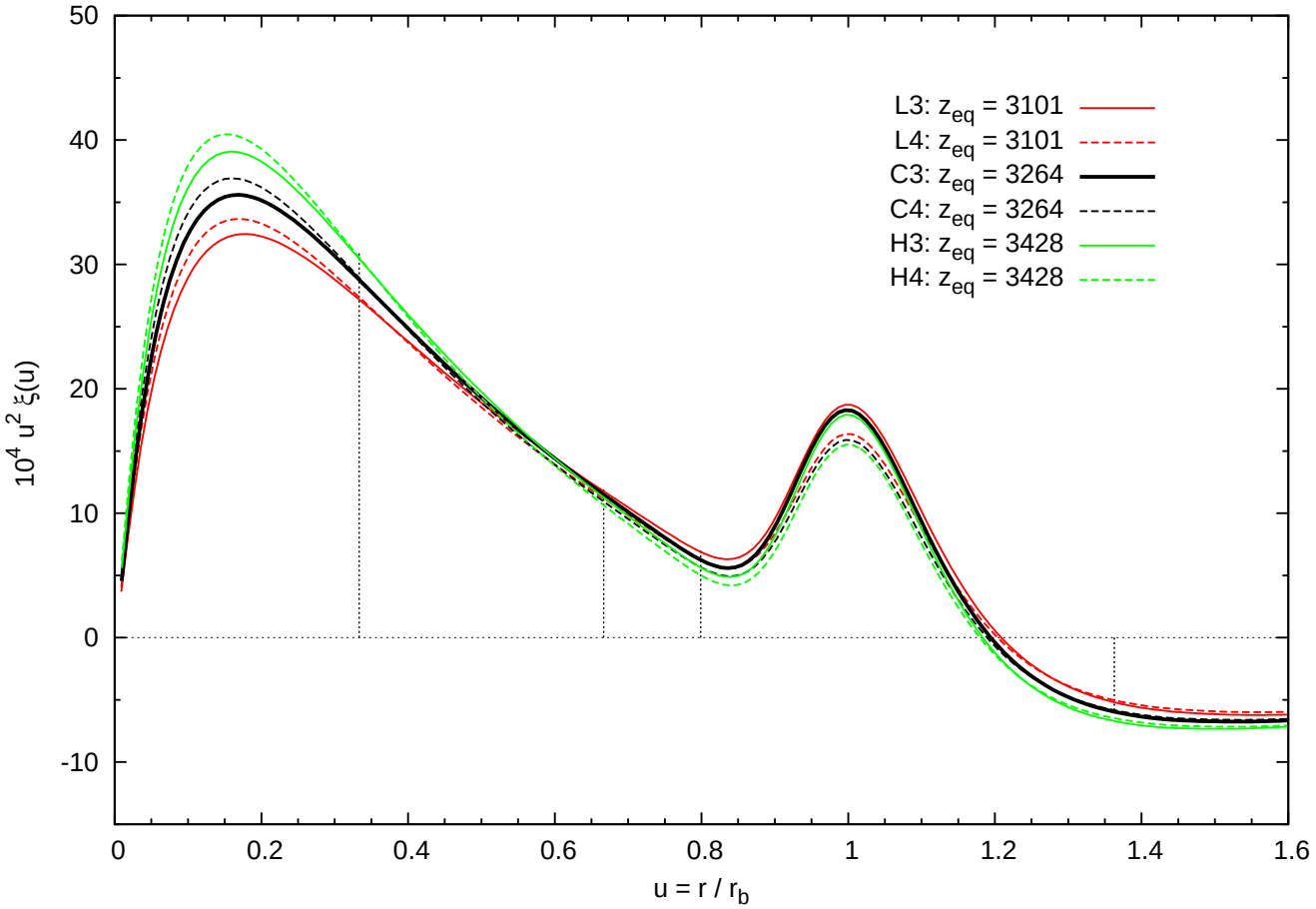

Figure 3. This figure shows the linear-theory matter correlation functions for the six example models from Table 1, now with the $x-$axis scaled so that $u = r/r_b$ and the BAO bump is at $u = 1$. The ordinate is $10^4 u^2 \xi(u)$. Models with $N_{\rm eff} = 3.04$ are solid lines; models with $N_{\rm eff} = 4.04$ are dashed lines. The thick solid line is model C3 ; the H and L models are respectively higher/lower around $u \sim 0.2$. Vertical dotted lines illustrate chosen integration limits u_1, u_2, u_3, u_4 as used in Eq. (8).

tion and amplitude to broad-band systematic errors in the observed $\xi(u)$.

The denominator of Eq. 8 is mainly sensitive to the broad-band large-scale power at $k \lesssim 0.1\,h\,{\rm Mpc}^{-1}$, which as above depends on the turnover scale in the matter power spectrum. If we measured this in a fixed range of Mpc or $h^{-1}\,$Mpc, this would depend on quantities such as Ω_{cb} and w, which would seriously degrade our ability to measure f_b; but since we chose our mid-scale power estimate as a fixed *fraction* of the BAO length rather than a fixed range in $h^{-1}\,$Mpc, this mostly cancels the dependence on low-redshift parameters such as Ω_{cb}, Ω_k and w; the broad-band shape of $\xi(u)$ at $0.2 < u < 0.8$ depends almost entirely on $z_{\rm eq}$ and n_s, which are already well constrained by the CMB. Therefore, we anticipate that W_b should depend mainly on f_b and only weakly on $z_{\rm eq}$.

To quantify this, we evaluated the ratio W_b for our six models, and the results are given in the last column of Table 1: the table shows that W_b is close to 0.61 for all three $N_{\rm eff} = 3.04$ models, and close to 0.56 for all three $N_{\rm eff} = 4.04$ models, consistent with our expectations above. The dependence of W_b on $z_{\rm eq}$ is below 1% and nearly negligible, while adding a fourth neutrino species or equivalent reduces W_b by a factor close to 0.915 (i.e. 8.5% suppression) in each case. This reduction is slightly less than we would expect from linear scaling $W_b \propto f_b$, since our $N_{\rm eff} = 4.04$ models have f_b reduced by a factor $1.134^{-1} = 0.882$ relative to the corresponding $N_{\rm eff} = 3.04$ model. The probable explanation is that baryons, in addition to causing oscillations, also affect the broad-band shape of the power spectrum (Eisenstein & Hu 1998) by suppressing power on all scales smaller than the sound horizon. Therefore, reducing the baryon fraction slightly increases power on intermediate scales, and changes the broad-band shape of $\xi(u)$, which slightly counteracts the reduction in the bump area.

The conclusion is that, *if* galaxy bias is scale-independent on large scales and the area of the BAO peak is conserved under non-linear evolution (or can be recovered by reconstruction methods), then measurements of W_b can offer a potential new probe of $N_{\rm eff}$. Estimates from large numerical simulations could be used to test these assumptions, and possibly attempt to correct for any resulting biases.

The largest current redshift surveys provide a $\sim 6\sigma$ detection of the BAO peak (Anderson et al 2012), which would translate to approximately 16 percent uncertainty in W_b; this is twice as large as the 8.5 percent shift predicted above for $N_{\rm eff} \sim 4$, so at present the precision on $N_{\rm eff}$ looks uncompetitive with other methods. However, future next-generation large redshift surveys can potentially offer a large improvement, and thus an interesting test of $N_{\rm eff}$ which is complementary to the better-known methods from the CMB and nucleosynthesis.

3.3 Effect of Planck data

Most of this paper studies models with parameter choices based on the WMAP-9 cosmological parameter results (Hinshaw et al 2012); the C3 model is near the best-fit, and L and H models have $z_{\rm eq}$ shifted by $\pm 1.5\sigma$ in WMAP units. After this paper was nearly completed, the first *Planck* cosmology data release occurred in 2013 March. While there are many interesting consequences for inflation and the early universe, for the present purposes, two results are most notable: firstly concerning $N_{\rm eff}$, the evidence for $N_{\rm eff} > 3.04$ has generally weakened (Ade et al 2013), but the strength of this conclusion is somewhat dependent on the choice of additional data sets.

The fit ΛCDM + varying $N_{\rm eff}$ to the dataset "*Planck* + WMAP polarisation + high-L + BAO" (the right column of Table 10 of Ade et al 2013) gives $N_{\rm eff} = 3.30 \pm 0.26$, which is 1σ above the standard value and excludes $N_{\rm eff} = 4.04$ at the 2.8σ level. However, there remains the well-publicised tension that *Planck* with vanilla ΛCDM (and $N_{\rm eff} = 3.04$) prefers a value of $H_0 \approx 67.8 \pm 0.8\,{\rm km\,s^{-1}\,Mpc^{-1}}$, which is below the 2σ range given by recent local measurements (Riess et al 2011; Freedman et al 2012). There are many possible explanations, but this H_0 tension can be ameliorated by increasing $N_{\rm eff}$: e.g. fitting *Planck* + H_0 data allowing variable $N_{\rm eff}$ gives $H_0 = 72.1 \pm 1.9\,{\rm km\,s^{-1}\,Mpc^{-1}}$ and $N_{\rm eff} = 3.62 \pm 0.25$, i.e. 2.2σ above the standard $N_{\rm eff}$. In summary, $N_{\rm eff} \sim 4.0$ is somewhat disfavoured by *Planck*, but a value of $N_{\rm eff} \sim 3.5$ is completely allowed or perhaps even preferred by combining all current data. There are interesting possible models with extra relativistic species other than neutrinos leading to $N_{\rm eff} \sim 3.5$ (e.g. Weinberg 2013).

Secondly, concerning $z_{\rm eq}$ and Ω_{cb}, the *Planck* data imply values somewhat higher than WMAP; for the vanilla ΛCDM model, fits to *Planck*+BAO data give $z_{\rm eq} = 3366 \pm 39$ and $\Omega_{cb} = 0.307 \pm 0.01$ (and $h = 0.678 \pm 0.008$ for standard $N_{\rm eff}$). The *Planck* constraints on $z_{\rm eq}$ are especially robust: in the many extensions of ΛCDM considered by the *Planck* team, the bounds $3150 \leqslant z_{\rm eq} \leqslant 3500$ are generic, i.e. values outside this range are excluded at $> 2\sigma$ for all of the added-parameter models and data combinations. (Clearly, still more complicated models with even more non-vanilla parameters might widen this range; but there appears little motivation at present for adding two or more new parameters beyond the basic six).

Comparing to our models above, the *Planck* central value $z_{\rm eq} \simeq 3366$ is near the mid-point between our model pairs C and H above, but slightly closer to H. Our two L models ($z_{\rm eq} = 3101$) are now firmly excluded by *Planck*, at around the 5σ level for the base model or 3σ for extended models. Also, *Planck* prefers $\omega_b \simeq 0.0221$ which is just 2 percent below our default; and $n_s \simeq 0.961$ which is nearly identical. Thus, while *Planck* has narrowed the allowed range of $z_{\rm eq}$ and $N_{\rm eff}$, our models C3/C4/H3/H4 approximately bracket the range of $z_{\rm eq}$ and $N_{\rm eff}$ allowed by *Planck*; and the main conclusions of this paper regarding the BAO amplitude are essentially unaffected.

4 CONCLUSIONS

We have shown that a measurement of the BAO peak amplitude via the observable W_b in Eq. 8 may provide an interesting measurement of the cosmic baryon fraction; this observable has been constructed so as to cancel galaxy bias, non-linearity and dark energy effects to leading order, thus being sensitive mostly to f_b.

Comparing this BAO-based measurement to the measurement of (approximately) $f_b X_{\rm rad}$ from the CMB then gives an interesting probe of $N_{\rm eff}$; this is largely complementary to the better-known method based on fitting the CMB damping tail. Here, the key inputs required from the CMB are constraints on $z_{\rm eq}$ and ω_b. Assuming standard gravity and standard recombination, these two parameters are very robust against extra-parameter extensions to vanilla ΛCDM.

There are two main assumptions used here: firstly that galaxy bias is nearly scale-independent on the large scales between $30 < r < 120\,h^{-1}\,{\rm Mpc}$, and secondly that the area (not height) of the BAO bump is conserved during the non-linear evolution of structure. Both of these assumptions are reasonably well-motivated, but much more detailed numerical simulations would be needed to see how well these approximations are expected to hold in practice.

A measurement of W_b to useful precision will require a substantial advance on current data: the current precision on the BAO bump area is around 16%, while we would need to reach around 3% to get a useful distinction between

$N_{\rm eff} = 3$ or 4; this appears a challenging proposition. However, given that the CMB temperature measurements are now approaching the limits set by cosmic variance and foregrounds, other independent probes of $N_{\rm eff}$ are highly desirable, and the test here should become feasible at no extra cost from planned next-generation BAO redshift surveys.

ACKNOWLEDGEMENTS

We thank the anonymous referee for helpful comments which significantly clarified this paper.

We acknowledge the use of WMAP data from the Legacy Archive for Microwave Background Data Analysis (LAMBDA) at GSFC (lambda.gsfc.nasa.gov), supported by the NASA Office of Space Science.

REFERENCES

Abazajian K.N., Acero M.A., Agarwalla S.K. et al, 2012. (arXiv:1204.5379)
Ade P.A.R., Aghanim N., Armitage-Caplan C. et al, Planck Collaboration XVI, 2013, A&A in press (arXiv:1303.5076)
Anderson L., Aubourg E., Bailey S. et al, 2012, MNRAS, 427, 3435.
Angulo R.E., Baugh C.M., Frenk C.S., Lacey C.G., 2008, MNRAS, 383, 755.
Bashinsky S. & Seljak U., 2004, Phys. Rev. D, 69, 083002.
Bassett B.A. & Hlozek R., 2010, in "Dark Energy", ed P. Ruiz-Lapuente, Cambridge Univ. Press, Cambridge, p. 246
Baugh C.M., 2013, PASA, 30, E30.
Beutler F., Blake C., Colless M. et al, 2011, MNRAS, 416, 3017.
Blake C., Davis T., Poole G. et al, 2011, MNRAS, 415, 2892
Bond J.R., Efstathiou G., 1984, ApJ, 285, L45
Cole S., Percival W.J., Peacock J.A. et al, 2005, MNRAS, 362, 505.
Dodelson, S., 2011, Int. J. Mod. Phys. D, 20, 2749. (arXiv:1112.1320)
Eisenstein D.J. & Hu W., 1998, ApJ, 496, 605.
Eisenstein D.J., Zehavi I., Hogg D. et al, 2005, ApJ, 633, 560.
Eisenstein D.J, Seo H., Sirko E., Spergel D.N., 2007, ApJ, 664, 675.
Eisenstein D.J, Seo H., White M., 2007, ApJ, 664, 660.
Fixsen D.J., 2009, ApJ, 707, 916.
Freedman W.L., Madore B.F., Scowcroft V., Burns C., Monson A., Persson S.E., Seibert M., Rigby J., 2012, ApJ, 758, 24.
Giusarma E., de Putter R., Ho S., Mena O., 2013, Phys. Rev. D, 88, 063515.
Hinshaw G., Larson D., Spergel D.N. et al, 2012, ApJS, 208, 19
Hou Z., Reichardt C.L., Story K.T. et al, 2012, preprint (arXiv:1212.6267)
Hou Z., Keisler R., Knox L., Millea M., Reichardt C., 2013, Phys.Rev.D., 87, 083008.
Hu W. & Sugiyama N., 1996, ApJ, 471, 542.
Hu W., Fukugita M., Zaldarriaga M., Tegmark M., 2001, ApJ, 549, 669.
Jimenez R., Verde L., Peiris H., Kosowsky A., 2004, Phys. Rev. D, 70, 3005.
Joudaki, S., 2013, Phys. Rev. D, 87, 083523.
Jungman, G., Kamionkowski M., Kosowsky A., Spergel D., 1996, PRD, 54, 1332.
Keisler R., Reichardt C.L., Aird K.A. et al, 2011, ApJ, 743, 28.
Komatsu E., Smith K., Dunkley J. et al, 2011, ApJS, 192, 18.
Mangano G., Miele G., Pastor S., Pinto T., Pisanti O., Serpico P.D., 2005, Nucl. Phys. B, 729, 221.
Mangano G., Serpico P.D., 2011, Phys. Lett. B, 701, 296.
Meiksin A., White M. & Peacock J.A., 1999, MNRAS, 304, 851.
Orban C., Weinberg D.H., 2011, Phys. Rev. D, 84, 063501.
Page L., Nolta M.R., Barnes C. et al, 2003, ApJS, 148, 233.
Peebles P.J.E. & Yu J.T, 1970, ApJ, 162, 815.
Padmanabhan N., Xu X., Eisenstein D.J., Scalzo R., Cuesta A.J., Mehta K.T., Kazin E., 2012, MNRAS, 427, 2132.
Percival W.J., Sutherland W., Peacock J.A. et al, 2002, MNRAS, 337, 1068.
Percival W.J., Reid B.A., Eisenstein D.J. et al, 2010, MNRAS, 401, 2148.
Pettini, M. & Cooke, R., 2012, MNRAS, 425, 2477.
Riemer-Sorensen S., Parkinson D., Davis T.M., 2013a, PASA, 30, E029.
Riemer-Sorensen S., Parkinson D., Davis T.M., 2013b, preprint (arXiv:1306.4153)
Riess A.G., Macri L., Casertano S. et al, 2011, ApJ, 730, 119.
Seo H-J., Eisenstein D.J., 2007, ApJ, 665, 14.
Seo H-J., Siegel E.R., Eisenstein D.J., White M., 2008, ApJ, 636, 13.
Seo H-J., Eckel J., Eisenstein D.J. et al, 2010, ApJ, 720, 1650.
Seo H-J., Ho S., White M. et al, 2012, ApJ, 761, 13.
Sievers J.L., Hlozek R., Nolta M.R. et al, 2013, JCAP, 10, 60.
Steigman G., Schramm D.N., Gunn J.E., 1977, Phys. Lett. B, 66, 202.
Story K.T., Reichardt C.L., Hou Z. et al, 2013, ApJ, 799, 86.
Sutherland W., 2012, MNRAS, 426, 1280.
Weinberg D.H., Mortonson M.J., Eisenstein D.J., Hirata C., Reiss A.G., Rozo E., 2013, Phys. Rep., 530, 87.
Weinberg, S., 2013, Phys. Rev. Lett., 110, 241301.

APPENDIX A: PARAMETER DEPENDENCE OF CMB PEAKS AND BAOS

In this section we give some accurate approximations for the dependence of CMB acoustic scale and BAO distance ratios on cosmological parameters, especially $z_{\rm eq}$ and Ω_{cb} used as basic parameters above. This helps to understand the parameter choices in Table 1, and the resulting shifts in BAO bump position observed in § 3.2.

Firstly, we find that a very good approximation to the CMB acoustic wavenumber ℓ_* for models fairly close to standard ΛCDM is

$$\ell_* \simeq 301.9 \left(\frac{1+z_{\rm eq}}{3201}\right)^{-0.25} \left(\frac{\Omega_{cb}}{0.270}\right)^{0.1} \left(\frac{1-f_\nu}{0.995}\right)^{0.4} (1+1.6\,\Omega_k)\,[1-0.11(1+w)] \tag{A1}$$

where $f_\nu \equiv \Omega_\nu/(\Omega_{cb}+\Omega_\nu)$, and this allows for small neutrino mass, weak curvature and constant $w \neq -1$. (This is for $\omega_b = 0.0226$; however, changing to the Planck value $\omega_b = 0.02215$ gives only around 0.1 percent reduction in ℓ_*). This has almost negligible dependence on $N_{\rm eff}$, since varying $N_{\rm eff}$ (at fixed $z_{\rm eq}, \Omega_{cb}$ as above) results in both $r_s(z_*)$ and $D_A(z_*)$ shrinking by a factor very close to $X_{\rm rad}^{-0.5}$, but these cancel almost exactly in ℓ_*.

Since ℓ_* is measured to high precision ≈ 0.2 percent by WMAP+ACT+SPT, if we vary $z_{\rm eq}$ (as in the L/H models in Table 1 above), then to remain consistent with CMB data we must adjust other parameter(s) to preserve ℓ_*. Given our assumption of flat Λ models and minimal neutrino mass in § 3, the only available parameter above is Ω_{cb}. Forcing a 5% reduction in $z_{\rm eq}$ (as chosen for models L3/L4) requires a 12% reduction in Ω_{cb} to keep ℓ_* the same as the baseline model C3; this corresponds to an increase in h by 3.6% (at fixed $N_{\rm eff}$). Shifts from C to H models are basically the opposite of this. We note one counter-intuitive feature: when varying parameters to conserve ℓ_*, it turns out that h changes in the *opposite* sense to $z_{\rm eq}$; this is distinct from the common case of fixing Ω_{cb} and varying h, when $1+z_{\rm eq}$ varies $\propto h^2$.

We can also understand the resulting shifts in the BAO bump location as follows: if we copy approximation (12) from Sutherland (2012) for low-redshift BAO ratios, which is

$$\frac{z\,r_s}{D_V(z)} \simeq 0.01868\,(1+\epsilon_V(z))\frac{E(\frac{2}{3}z)}{\sqrt{\Omega_{cb}}}\left(\frac{1+z_{\rm eq}}{3201}\right)^{0.25}\quad; \tag{A2}$$

here the LHS is a direct observable from a BAO survey at effective redshift z, $D_V(z)$ is the usual BAO dilation length (Eisenstein et al 2005), $E(z) \equiv H(z)/H_0$, and ϵ_V is a small cosmology-dependent correction term (Sutherland 2012), which is typically $\lesssim 0.05z^2$ and effectively negligible at modest redshift $z \lesssim 0.3$. Approximation A2 is accurate to $\lesssim 0.7\%$ at $z \leqslant 0.4$, comparable to the cosmic variance limit, and again this is almost independent of $N_{\rm eff}$. At low redshift, Eq. A2 is only weakly sensitive to additional non-vanilla parameters such as curvature and varying w via the $E(2z/3)$ term; this explains why low-redshift BAO observations provide a very robust constraint on Ω_{cb}.

In the limit $z \to 0$, the above simplifies to

$$\frac{r_s\,H_0}{c} \simeq \frac{0.01868}{\sqrt{\Omega_{cb}}}\left(\frac{1+z_{\rm eq}}{3201}\right)^{0.25}\quad. \tag{A3}$$

The LHS is equivalent to a hypothetical BAO measurement at $z = 0$; this is not strictly observable since cosmic variance prevents us measuring the BAO feature at $z \lesssim 0.1$; but it is a modest extrapolation from real low-z BAO surveys. The main point is since a galaxy redshift survey of course measures redshifts not distances, the apparent BAO bump "length" presented in $h^{-1}\,$Mpc units, as in Figure 2, is really measuring the "BAO velocity" $H_0\,r_s$ in units of $100\,{\rm km\,s^{-1}}$. Although this quantity contains h, in the case of varying $N_{\rm eff}$ this gets cancelled: if we vary $N_{\rm eff}$ while holding fixed $z_{\rm eq}$ (as appropriate for fitting CMB data), then h and r_s both depend on the radiation density as $X_{\rm rad}^{1/2}$ and $X_{\rm rad}^{-1/2}$ respectively; so their product is almost independent of $X_{\rm rad}$ and only depends on the dimensionless parameters $z_{\rm eq}$ and Ω_{cb}, plus a very weak dependence on ω_b which is negligible at the current level of accuracy. Therefore, the observed velocity scale of the BAO feature at low redshift is primarily measuring Ω_{cb}, not h, which explains why the BAO feature does not shift between the 3 and 4 neutrino model pairs in § 3.2.

Since all of the approximations above are nearly independent of $N_{\rm eff}$, this was the rationale for choosing $z_{\rm eq}$ and Ω_{cb} as two of the basic parameters: observations of CMB and BAOs give us direct constraints on $z_{\rm eq}$ and Ω_{cb}, nearly independent of $N_{\rm eff}$. These two directly give a constraint on $h/\sqrt{X_{\rm rad}}$ from Eq. 5, but give almost no ability to measure h, $X_{\rm rad}$ separately; this explains why WMAP+BAO alone currently have very weak leverage on $N_{\rm eff}$, unless further dimensionful data such as H_0 or t_0 is added.

Finally, the fact that Ω_{cb} appears with a -0.5 power in Eq. A3 explains why the BAO feature shifts to smaller (larger) velocity scale for the models H (L) above.

This paper has been typeset from a TEX/ LATEX file prepared by the author.